

Controlling the Dipole Blockade and Ionization Rate of Rydberg Atoms in Strong Electric Fields

Markus Stecker,¹ Raphael Nold,¹ Lea-Marina Steinert,¹ Jens Grimm,¹ David Petrosyan,^{1,2}
József Fortágh,¹ and Andreas Günther^{1,*}

¹*Center for Quantum Science, Physikalisches Institut, Eberhard Karls Universität Tübingen,
Auf der Morgenstelle 14, D-72076 Tübingen, Germany*

²*Institute of Electronic Structure and Laser, FORTH, GR-70013 Heraklion, Crete, Greece*



(Received 21 May 2019; accepted 28 July 2020; published 31 August 2020)

We study a hitherto unexplored regime of the Rydberg excitation blockade using highly Stark-shifted, yet long-living, states of Rb atoms subject to electric fields above the classical ionization limit. Such states allow tuning the dipole-dipole interaction strength while their ionization rate can be changed over 2 orders of magnitude by small variations of the electric field. We demonstrate laser excitation of the interacting Rydberg states followed by their detection using controlled ionization and magnified imaging with high spatial and temporal resolution. Our work reveals new possibilities to engineer the interaction strength and dynamically control the ionization and detection of Rydberg atoms, which can be useful for realizing and assessing quantum simulators that vary in space and time.

DOI: [10.1103/PhysRevLett.125.103602](https://doi.org/10.1103/PhysRevLett.125.103602)

Atoms excited to highly polarizable Rydberg states can exhibit strong interactions and long-range correlations, which makes them promising systems for quantum information processing [1–3] and quantum simulations [4,5]. The interatomic interactions can be of long-range dipole-dipole or shorter range van der Waals type [6], often manifested in the experiments through the so-called Rydberg blockade, i.e., suppression of laser excitation of more than one Rydberg atom within a certain blockade volume.

The efficiency of the blockade and the fidelity of blockade-based quantum gates depend on the strength of the Rydberg-Rydberg interactions [7–9]. A tunable interaction potential is also highly desirable for quantum simulators [4,5]. Following the first demonstrations of the Rydberg blockade [10,11], much effort has been devoted to enhancement and tuning of the interatomic interactions, e.g., by shifting the atomic Rydberg states with a weak electric field to a Förster resonance [12–14], using states with near resonant dipole-dipole interactions at zero field [15], employing the ac Stark shifts of the Rydberg states [16], and using rotary echo [17] or weak static electric fields [18–20]. Rydberg blockade between two individual atoms [21,22] and two-qubit gates and entanglement have been achieved [23–26], and single collective Rydberg excitations in blockaded atomic ensembles have been observed [27–29]. Finally, simulations of quantum Ising models with atoms in a lattice or arrays of microtraps have been demonstrated [30–37]. Spatially resolved measurement of the Rydberg blockade has been studied with separate excitation areas [38,39], quantum gas microscopes [30,31], interaction enhanced imaging [40,41] and direct imaging by field ionization [42–45].

In this work, we investigate for the first time the dipole-dipole interactions between Rydberg atoms in a strong static electric field close to the classical ionization limit, which hitherto deemed inapplicable for such experiments. Yet, we identify highly Stark-shifted states with static but tunable dipole moments and low ionization rates suitable for observing correlations stemming from the Rydberg blockade. We vary the interatomic interaction strength by small changes in the external electric field and observe Rydberg blockade of different strength and range. We note that excitation blockade of Rydberg states having permanent and tunable dipole moments has not been achieved before. Furthermore, we demonstrate a novel detection scheme in which the atoms in a long-living Rydberg state are adiabatically transferred to a state with a strongly enhanced ionization rate. Spatially and temporally resolved detection of individual Rydberg atoms is then achieved by imaging the ions with our unique high resolution ion microscope [46].

Our experimental setup is illustrated in Fig. 1(a). It consists of a vacuum chamber with a standard magneto-optical trap (MOT) for ⁸⁷Rb atoms and an ion microscope. The MOT contains up to 10⁷ atoms at temperature $T \simeq 150 \mu\text{K}$ and peak density $D \simeq 4 \times 10^{10} \text{ cm}^{-3}$. Two extractor electrodes can generate the desired, nearly homogeneous electric field at the position of the atoms in the MOT. The atoms are excited to the Rydberg state by a two-photon transition from the $5S_{1/2}$ ground state via the near-resonant intermediate $5P_{3/2}$ state [see Fig. 1(b)]. The lower transition at a wavelength around 780 nm is provided by the continuous MOT cooling laser, while the upper transition at

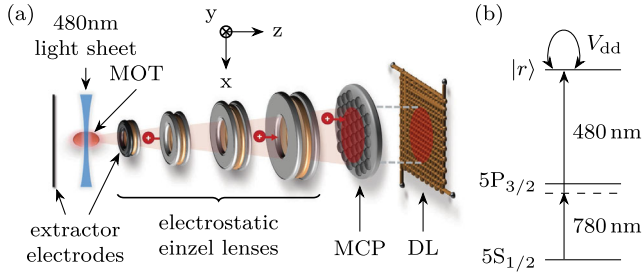


FIG. 1. (a) Experimental setup for Rydberg excitation of atoms followed by spatially resolved ion detection. Atoms in a magneto-optical trap (MOT) are excited to the Rydberg state in the overlap region of the 780 nm MOT laser and the 480 nm laser light sheet. Field ionized Rydberg atoms are imaged via electrostatic einzel lenses onto a multichannel plate (MCP) and electronically detected via a delay line anode (DL) with single ion sensitivity and high temporal and spatial resolution. (b) Rydberg excitation scheme for ^{87}Rb atoms with a two-photon transition from the $5S_{1/2}$ ground state to a high lying Rydberg state $|r\rangle$ via the intermediate $5P_{3/2}$ state. The atoms in state $|r\rangle$ interact with each other via the dipole-dipole potential V_{dd} .

around 480 nm is driven by a pulsed laser stabilized with a wavelength meter (HighFinesse WS8-2). This blue laser beam is directed along x , perpendicular to the electric field of the extractor electrodes and the optical axis of the ion imaging, and is focused to a light sheet with beam waists of $w_z \simeq 4.5 \mu\text{m}$ and $w_y \simeq 40 \mu\text{m}$ in order to limit the excitation depth in the z direction of the ion imaging. The spatially resolved detection of ions outside of the MOT is performed by an ion microscope composed of four consecutive electrostatic lenses and a multichannel plate in conjunction with a delay line anode for electronic readout of the individual ion positions and time stamps [see Fig. 1(a)]. The magnification of the ion microscope is around 1000, resulting in an imaging area of $40 \mu\text{m}$ diameter; further details of the experimental setup can be found in Ref. [46].

The energy landscape of highly Stark-shifted Rydberg atoms exhibits an intricate form [47] and is governed by strongly varying line broadenings due to ionization. From our numerical calculations [48] using a complex absorbing potential (CAP) [49–51], we identify several states with small ionization rates and different dipole moments. In Fig. 2(a) we show the calculated Stark spectrum and ionization rates around the (unperturbed) $43S_{1/2}$ state of ^{87}Rb with the electric field in the interval of 126–129 V/cm around the classical ionization threshold at 127.2 V/cm. We choose this field region because it features multiple resonance lines that undergo a strong change in ionization rate, from long living to strongly ionizing, within a small interval of the electric field. The numerically calculated laser excitation spectrum of the Stark-shifted Rydberg states is shown in Fig. 2(b).

To experimentally verify the theoretically predicted ionization rates, we excite the atoms to the Rydberg states

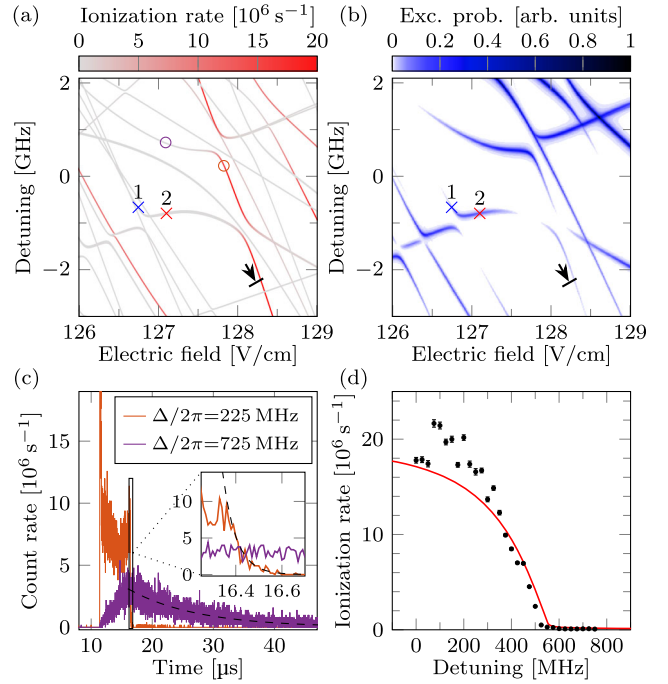


FIG. 2. (a) Numerically calculated Stark spectrum of ^{87}Rb atoms near the classical ionization threshold at 127.2 V/cm, with the detuning relative to the unperturbed $43S_{1/2}$ state. Ionization rates of the individual Stark lines range from nonionizing (gray) to strongly ionizing (red). Crosses indicate the strongly (1) and weakly (2) interacting resonances used in the Rydberg blockade experiment of Fig. 3. The arrowhead with a delimiter mark indicates the ionizing state that the Rydberg state is transferred to for the blockade measurements. (b) Excitation strength of Rydberg resonances calculated for the laser polarizations and the dipole matrix elements of the corresponding optical transitions, starting from the $5S_{1/2}$ ground state [see Fig. 1(b)]. (c) Examples of the ion signal decay, for the two resonances indicated by open circles in panel (a), for the extraction of Rydberg state ionization rates. (d) Measured (black dots) and calculated (solid red line) ionization rates along the Stark line with open circles in panel (a).

lying on one of the Stark lines at different electric fields, with the corresponding detuning of the blue laser, and simultaneously detect the arrival times of the ions reaching the detector. With the MOT magnetic field and lasers continuously on, the blue laser is pulsed for 1–5 μs , each pulse typically yielding 1–30 ions, depending on the transition strength and pulse duration. We repeat the excitation pulse several thousand times to derive a histogram of the ion arrival times. We then determine the ionization rate of the state from the decay of the ion signal after the end of the excitation pulse, as illustrated in Fig. 2(c). We note that radiative decay to lower states [52] and population redistribution by black body radiation [53] can alter the ionization rate of the Rydberg atoms. Yet, we do not expect significant contributions of these processes, having typically rates of a few tens of kHz, as

compared to our observed ionization rates in the MHz range. As seen in Fig. 2(d), the experimental data are in good agreement with the results of numerical calculations performed for a zero temperature environment. Deviations between theory and experiment may be attributed to the fact that the free parameter of the CAP potential was optimized for a broad spectral range and not for a single resonance [48].

Our results thus demonstrate that by a small variation of the electric field the ionization rate of the atomic Rydberg states can be precisely tuned in a wide interval, from a few tens of kHz up to several MHz, which can facilitate the temporally and spatially resolved detection of Rydberg atoms. We can excite the atoms to a long-living Rydberg state and then adiabatically transfer them to a state with a well-defined ionization rate by a small change of the electric field. Typically, we change the electric field by about 1 V/cm within 1 μ s. Traditionally, Rydberg atoms are ionized by simply switching on, or ramping up, the electric field to a much higher value. In contrast, our approach permits a high degree of control of ionization. We can dynamically tune the ionization rate to be, on the one hand, strong enough for the atoms not to move or decay significantly while they are ionized, and, on the other hand, low enough to avoid saturation of the ion detector. Moreover, our method permits the reversal of the ionization rate from strong to weak by an adiabatic change of the electric field. This is virtually impossible when ionizing by switching on a strong field which results in rapid redistribution of the population of the initial Rydberg state over many Stark-shifted states [54].

We now turn to the study of Rydberg blockade in the atomic ensemble. We choose the electric field values and the corresponding frequency of the blue laser to resonantly excite slowly ionizing Rydberg states characterized by different dipole moments and thereby different strengths of the interatomic interactions. Specifically, we selectively address a single Stark line at two positions, 1 and 2, as indicated in Figs. 2(a) and 2(b). Resonance 1 corresponds to the electric field of $F = 126.75$ V/cm and a laser detuning $\Delta/2\pi = -664$ MHz (relative to the unperturbed $43S_{1/2}$ state), while resonance 2 corresponds to $F = 127.1$ V/cm and $\Delta/2\pi = -794$ MHz. The dipole moment p_z of a Stark-shifted state with energy $E(F)$ in an electric field F can be determined from the slope of the resonance line $p_z = -dE(F)/dF$. For the first resonance with the large energy slope we obtain the dipole moment $p_z \simeq 2000ea_0 = 1.69 \times 10^{-26}$ Cm, which should lead to a strong dipole-dipole interaction with the coefficient $C_3/2\pi \simeq 3.9$ GHz μm^3 (see below) and thereby well-pronounced blockade. In contrast, the small slope around the second resonance results in a smaller dipole $p_z \simeq -210ea_0 = -1.76 \times 10^{-27}$ Cm and an interaction coefficient $C_3/2\pi \simeq 42$ MHz μm^3 , leading to much weaker excitation blockade.

For the spatially resolved detection of Rydberg atoms, the blue laser pulse excites the atoms to slowly ionizing Rydberg states. We set the duration of the pulse to $\tau = 5$ μ s for resonance 1 with weaker two-photon excitation strength, and to $\tau = 1$ μ s for resonance 2 with stronger excitation strength [see Fig. 2(b)]. Following the excitation, the voltage at the extractor electrodes is ramped up to about $F = 128.3$ V/cm within 1 μ s using a high voltage switch. This transfers the Rydberg atoms to a rapidly ionizing state, as indicated by the arrowhead marker in Fig. 2(a). The ions are detected by our ion optics setup which records the time of flight and positions of the ions hitting the detector. The magnification of the ion-optical system is set to 1129. Each excitation-detection cycle typically yields 2–8 ions and is repeated up to 3×10^5 times to accumulate good statistics.

After each excitation and spatially resolved ion detection, we calculate the two-dimensional second order correlation function

$$g^{(2)}(u, v) = \frac{\langle\langle f(x+u, y+v)f(x, y) \rangle\rangle_{x,y}}{\langle\langle f(x+u, y+v) \rangle\rangle_{x,y} \langle\langle f(x, y) \rangle\rangle_{x,y}}, \quad (1)$$

where u, v are the displacements, $f(x, y) = \sum_{i=1}^N \delta(x - x_i)\delta(y - y_i)$ is the detector function with the coordinates x_i and y_i of the N incoming ions on the detector, and $\langle\langle \cdot \rangle\rangle_{x,y}$ denotes the average over the x and y positions. The correlation results for the individual cycles are summed up. In order to compensate for the spatially inhomogeneous excitation probability (due to inhomogeneous laser power) and the finite detector size, the result is normalized to the correlation function calculated from all events at once. In the inset of Fig. 3(a) we show an example of such a measured correlation function for the excitation of the strongly interacting Rydberg state. The correlation function has a reduced value $g^{(2)}(u, v) < 1$ in a certain blockade region $\sqrt{u^2 + v^2} < r_b \sim 10$ μm around the origin ($u, v = 0$) with no apparent anisotropy. Hence, in the vicinity of a Rydberg excited atom, the probability of another excitation is strongly suppressed, which is a clear manifestation of the Rydberg blockade.

In Fig. 3(a) we show the correlation function $g^{(2)}(r)$ versus distance r between the Rydberg excitations as obtained by radial binning and angle averaging the two-dimensional correlation function $g^{(2)}(u, v)$. At large distances, $r > r_b$, there are no correlations between the Rydberg excitations, corresponding to $g^{(2)}(r) \simeq 1$. At smaller distances, $r \lesssim r_b$, the suppression of multiple Rydberg excitations, $g^{(2)}(r) < 1$, signifies the blockade correlations. Clearly the blockade strength and distance are much larger for the strongly interacting Rydberg state (resonance 1) than for the weakly interacting state (resonance 2).

The dipole-dipole interaction potential between pairs of atoms in the Rydberg state with a permanent dipole moment p_z along the \hat{z} direction is given by

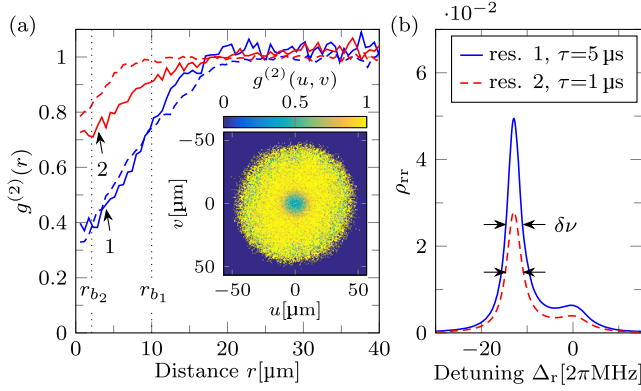


FIG. 3. (a) Correlation function $g^{(2)}(r)$ versus distance r , as obtained from the experimental ion measurements for the Rydberg excitation of resonances 1 (thick solid blue line) and 2 (thick solid red line). The corresponding results from the numerical Monte Carlo simulations are plotted with dashed lines of the same color. The inset shows the experimental two-dimensional correlation function $g^{(2)}(u, v)$ for resonance 1. (b) Excitation probability ρ_{rr} of Rydberg state $|r\rangle$ for a three-level atom versus detuning Δ_r of the blue laser, as obtained from numerical solution of the density matrix equations with the following parameters: The cw red laser acts on the lower atomic transition $5S_{1/2} \leftrightarrow 5P_{3/2}$ with Rabi frequency $\Omega_{780}/2\pi = 7.4$ MHz and detuning $\Delta_{780}/2\pi = 12$ MHz, while the blue laser acting on the upper transition $5P_{3/2} \leftrightarrow |r\rangle$ with Rabi frequency $\Omega_{480}/2\pi = 0.3, 0.5$ MHz is pulsed for time $\tau = 5, 1 \mu\text{s}$ for resonance 1, 2, respectively. Decay rates of the intermediate and Rydberg states are $\Gamma_{5P}/2\pi = 6$ MHz and $\Gamma_r/2\pi = 30$ kHz, and the dephasing rates for the corresponding transitions are $\gamma_{5P}/2\pi = 0.55$ MHz and $\gamma_r/2\pi = 1$ MHz. The Rydberg excitation linewidth is $\delta\nu \simeq 2\pi \times 3.8$ MHz for both resonances 1, 2.

$$V_{\text{dd}} = \hbar \frac{C_3}{r^3} (1 - 3 \cos^2 \theta), \quad (2)$$

where $C_3 \equiv p_z^2/(4\pi\epsilon_0\hbar)$ is the interaction coefficient referred to above, $r \equiv |\mathbf{r}|$ is the distance between the atoms, and θ is the angle between vectors \hat{z} and \mathbf{r} . We can estimate the blockade distance r_b as follows. The excitation volume is determined by the blue laser field which is a thin light sheet, $w_z \ll w_y$, oriented perpendicular to the strong electric field F of the ion extractor electrodes in the \hat{z} direction. We may therefore assume $\theta = \pi/2$ in Eq. (2). The blockade distance is then defined via $V_{\text{dd}}/\hbar \geq \delta\nu$ as the distance $r_b = (C_3/\delta\nu)^{1/3}$ at which the interaction-induced level shift of the Rydberg state $|r\rangle$ is equal to, or larger than, the excitation linewidth $\delta\nu$ of the atoms subject to near-resonant lasers. In Fig. 3(b) we show the spectra of Rydberg excitation of three-level atoms obtained by numerically solving the density matrix equations for the stated parameters. There, the main peaks at $\Delta_r \simeq -\Delta_{780}$ correspond to the direct two-photon excitation from the ground state $5S_{1/2}$, while the small peaks at $\Delta_r \simeq 0$ are due to incoherent two-step excitation through the nonresonantly

populated $5P_{3/2}$ state [55]. For both resonances 1 and 2, we obtain the Rydberg excitation linewidth $\delta\nu \simeq 2\pi \times 3.8$ MHz, leading to $r_b \simeq 10 \mu\text{m}$ for resonance 1, and $r_b \simeq 2.2 \mu\text{m}$ for resonance 2.

In Fig. 3(a) we compare the experimentally obtained correlations between the Rydberg excitations with the results of our numerical simulations. In the simulations, we place the atoms with the average density $D \simeq 0.04 \mu\text{m}^{-3}$ at random positions in a sufficiently large volume. The three-level atoms are driven by a spatially and temporally uniform red laser acting on the lower transition, and a pulsed blue laser, focused to a light sheet, acting on the upper transition, with the atomic parameters as in Fig. 3(b). The laser fields are in two-photon resonance with an unperturbed Rydberg level of the atoms, but the Rydberg level of each atom is shifted by the interaction with all the other Rydberg excited atoms, which translates into the corresponding detuning Δ_r of the laser. The Rydberg excitations at different positions are then obtained by Monte Carlo sampling of the excitation probabilities of the atoms [56–58]. After the excitation pulse, the Rydberg state atoms are assumed ionized and detected in the x, y plane by the ion detector. We take the ion detection efficiency $\eta = 0.7$ and a Gaussian position uncertainty with standard deviation $\sigma_{x,y} = 2.3 \mu\text{m}$ for resonance 1 and $\sigma_{x,y} = 1.2 \mu\text{m}$ for resonance 2. The larger position uncertainty for the former case is intended to model the thermal atomic motion during the longer $\tau = 5 \mu\text{s}$ excitation time. The correlation functions shown in Fig. 3(a) are obtained after averaging over 10^5 independent realizations of the dynamics of Rydberg excitations and detection in random atomic ensembles. The numerically obtained correlation functions are in reasonably good agreement with the corresponding experimental ones.

Note, that even for the strongly interacting case of resonance 1, the correlation function $g^{(2)}(r)$ does not reach zero for $r \rightarrow 0$. This is due to the finite thickness w_z of the excitation volume where the angular dependence and zeroes of the dipole-dipole potential V_{dd} partially mask the blockade. But even in perfectly 1D or 2D geometries, the Rydberg blockade due to the dipole-dipole potential $V_{\text{dd}} \propto r^{-3}$ is much “softer,” and the blockade distance is more uncertain, as compared to those for the van der Waals potential $V_{\text{vdW}} \propto r^{-6}$ [58]. Yet, to achieve comparable blockade distances in the van der Waals regime, Rydberg states with much higher principal quantum numbers (close to $n = 100$) will be required.

To conclude, we have shown that long-living Rydberg excitations and strong and tunable interatomic interactions can be observed with highly Stark-shifted states of atoms in strong electric fields. Our results open up the possibilities to realize quantum gates and simulations with Rydberg atoms in the strong field regime dominated by the long-range dipole-dipole interactions. In many experiments, the atoms are subject to strong or residual electric fields, especially in

chip-based quantum systems, where adsorbates on the surfaces play a crucial role [59–62]. Such experiments often strive to couple Rydberg atoms to surface based quantum systems, such as superconducting qubits or coplanar waveguide resonators [63–67], requiring the atoms to be brought close to the surface [68,69]. Then, the surface fields typically have to be compensated in all spatial directions by a set of electrodes, which can be challenging and cumbersome. Instead of trying to attain a zero field condition at the atomic position, we have shown in this work that the complicated “spaghetti region” of the Stark spectrum with its diversity of states can be seen as an advantage rather than annoyance, allowing for tailoring excitation, interaction, and ionization of Rydberg states. Strong and tunable dipole-dipole interactions can then be achieved at, compared to van der Waals driven interactions, much lower principal quantum numbers. The possibility to dynamically tune the interaction strength via small changes in the electric field, opens up new perspectives for Rydberg based quantum gates. Being able to precisely switch the dipole-dipole interaction on and off, may allow for precise timing of quantum gate operations between atoms without the need of transferring them by lasers to noninteracting lower states, which would otherwise reduce the gate fidelity [70]. Time-dependent interactions may also allow to investigate dynamically driven long-range interacting system and quenched dynamics in Rydberg quantum simulators [4,5,30–37].

This work was supported by the Deutsche Forschungsgemeinschaft through SPP 1929 (GiRyd). M. S. acknowledges financial support from Landesgraduiertenförderung Baden-Württemberg.

*a.guenther@uni-tuebingen.de

- [1] D. Jaksch, J. I. Cirac, P. Zoller, S. L. Rolston, R. Côté, and M. D. Lukin, *Phys. Rev. Lett.* **85**, 2208 (2000).
- [2] M. D. Lukin, M. Fleischhauer, R. Cote, L. M. Duan, D. Jaksch, J. I. Cirac, and P. Zoller, *Phys. Rev. Lett.* **87**, 037901 (2001).
- [3] M. Saffman, T. G. Walker, and K. Mølmer, *Rev. Mod. Phys.* **82**, 2313 (2010).
- [4] H. Weimer, M. Müller, I. Lesanovsky, P. Zoller, and H. P. Büchler, *Nat. Phys.* **6**, 382 (2010).
- [5] A. Browaeys and T. Lahaye, *Nat. Phys.* **16**, 132 (2020).
- [6] A. Reinhard, T. C. Liebisch, B. Knuffman, and G. Raithel, *Phys. Rev. A* **75**, 032712 (2007).
- [7] M. Saffman and T. G. Walker, *Phys. Rev. A* **72**, 022347 (2005).
- [8] X. L. Zhang, A. T. Gill, L. Isenhower, T. G. Walker, and M. Saffman, *Phys. Rev. A* **85**, 042310 (2012).
- [9] D. Petrosyan, F. Motzoi, M. Saffman, and K. Mølmer, *Phys. Rev. A* **96**, 042306 (2017).
- [10] D. Tong, S. M. Farooqi, J. Stanojevic, S. Krishnan, Y. P. Zhang, R. Côté, E. E. Eyler, and P. L. Gould, *Phys. Rev. Lett.* **93**, 063001 (2004).
- [11] K. Singer, M. Reetz-Lamour, T. Amthor, L. G. Marcassa, and M. Weidemüller, *Phys. Rev. Lett.* **93**, 163001 (2004).
- [12] T. Vogt, M. Viteau, J. Zhao, A. Chotia, D. Comparat, and P. Pillet, *Phys. Rev. Lett.* **97**, 083003 (2006).
- [13] A. Reinhard, K. C. Younge, T. C. Liebisch, B. Knuffman, P. R. Berman, and G. Raithel, *Phys. Rev. Lett.* **100**, 233201 (2008).
- [14] S. Ravets, H. Labuhn, D. Barredo, L. Béguin, T. Lahaye, and A. Browaeys, *Nat. Phys.* **10**, 914 (2014).
- [15] A. Reinhard, K. C. Younge, and G. Raithel, *Phys. Rev. A* **78**, 060702(R) (2008).
- [16] P. Bohlouli-Zanjani, J. A. Petrus, and J. D. D. Martin, *Phys. Rev. Lett.* **98**, 203005 (2007).
- [17] N. Thaicharoen, A. Schwarzkopf, and G. Raithel, *Phys. Rev. Lett.* **118**, 133401 (2017).
- [18] T. Vogt, M. Viteau, A. Chotia, J. Zhao, D. Comparat, and P. Pillet, *Phys. Rev. Lett.* **99**, 073002 (2007).
- [19] N. Thaicharoen, L. F. Gonçalves, and G. Raithel, *Phys. Rev. Lett.* **116**, 213002 (2016).
- [20] L. F. Gonçalves and L. G. Marcassa, *Phys. Rev. A* **94**, 043424 (2016).
- [21] E. Urban, T. A. Johnson, T. Henage, L. Isenhower, D. D. Yavuz, T. G. Walker, and M. Saffman, *Nat. Phys.* **5**, 110 (2009).
- [22] A. Gaëtan, Y. Miroshnychenko, T. Wilk, A. Chotia, M. Viteau, D. Comparat, P. Pillet, A. Browaeys, and P. Grangier, *Nat. Phys.* **5**, 115 (2009).
- [23] L. Isenhower, E. Urban, X. L. Zhang, A. T. Gill, T. Henage, T. A. Johnson, T. G. Walker, and M. Saffman, *Phys. Rev. Lett.* **104**, 010503 (2010).
- [24] T. Wilk, A. Gaëtan, C. Evellin, J. Wolters, Y. Miroshnychenko, P. Grangier, and A. Browaeys, *Phys. Rev. Lett.* **104**, 010502 (2010).
- [25] K. M. Maller, M. T. Lichtman, T. Xia, Y. Sun, M. J. Piotrowicz, A. W. Carr, L. Isenhower, and M. Saffman, *Phys. Rev. A* **92**, 022336 (2015).
- [26] H. Levine, A. Keesling, A. Omran, H. Bernien, S. Schwartz, A. S. Zibrov, M. Endres, M. Greiner, V. Vuletić, and M. D. Lukin, *Phys. Rev. Lett.* **121**, 123603 (2018).
- [27] T. M. Weber, M. Höning, T. Niederprüm, T. Manthey, O. Thomas, V. Guarrera, M. Fleischhauer, G. Barontini, and H. Ott, *Nat. Phys.* **11**, 157 (2015).
- [28] M. Ebert, M. Kwon, T. G. Walker, and M. Saffman, *Phys. Rev. Lett.* **115**, 093601 (2015).
- [29] J. Zeiher, P. Schauß, S. Hild, T. Macrì, I. Bloch, and C. Gross, *Phys. Rev. X* **5**, 031015 (2015).
- [30] P. Schauß, M. Cheneau, M. Endres, T. Fukuhara, S. Hild, A. Omran, T. Pohl, C. Gross, S. Kuhr, and I. Bloch, *Nature (London)* **491**, 87 (2012).
- [31] P. Schauss, J. Zeiher, T. Fukuhara, S. Hild, M. Cheneau, T. Macrì, T. Pohl, I. Bloch, and C. Gross, *Science* **347**, 1455 (2015).
- [32] H. Labuhn, D. Barredo, S. Ravets, S. de Léséleuc, T. Macrì, T. Lahaye, and A. Browaeys, *Nature (London)* **534**, 667 (2016).
- [33] H. Bernien, S. Schwartz, A. Keesling, H. Levine, A. Omran, H. Pichler, S. Choi, A. S. Zibrov, M. Endres, M. Greiner, V. Vuletić, and M. D. Lukin, *Nature (London)* **551**, 579 (2017).

- [34] V. Lienhard, S. de Léséleuc, D. Barredo, T. Lahaye, A. Browaeys, M. Schuler, L.-P. Henry, and A. M. Läuchli, *Phys. Rev. X* **8**, 021070 (2018).
- [35] E. Guardado-Sanchez, P. T. Brown, D. Mitra, T. Devakul, D. A. Huse, P. Schauß, and W. S. Bakr, *Phys. Rev. X* **8**, 021069 (2018).
- [36] A. Keesling, A. Omran, H. Levine, H. Bernien, H. Pichler, S. Choi, R. Samajdar, S. Schwartz, P. Silvi, S. Sachdev, P. Zoller, M. Endres, M. Greiner, V. Vuletić, and M. D. Lukin, *Nature (London)* **568**, 207 (2019).
- [37] A. Omran, H. Levine, A. Keesling, G. Semeghini, T. T. Wang, S. Ebadi, H. Bernien, A. S. Zibrov, H. Pichler, S. Choi, J. Cui, M. Rossignolo, P. Rembold, S. Montangero, T. Calarco, M. Endres, M. Greiner, V. Vuletić, and M. D. Lukin, *Science* **365**, 570 (2019).
- [38] C. S. E. van Ditzhuijzen, A. F. Koenderink, J. V. Hernández, F. Robicheaux, L. D. Noordam, and H. B. van Linden van den Heuvell, *Phys. Rev. Lett.* **100**, 243201 (2008).
- [39] T. J. Carroll, K. Claringbould, A. Goodsell, M. J. Lim, and M. W. Noel, *Phys. Rev. Lett.* **93**, 153001 (2004).
- [40] G. Günter, M. Robert-de-Saint-Vincent, H. Schempp, C. S. Hofmann, S. Whitlock, and M. Weidemüller, *Phys. Rev. Lett.* **108**, 013002 (2012).
- [41] G. Günter, H. Schempp, M. Robert-de Saint-Vincent, V. Gavryusev, S. Helmrich, C. S. Hofmann, S. Whitlock, and M. Weidemüller, *Science* **342**, 954 (2013).
- [42] A. Schwarzkopf, R. E. Sapiro, and G. Raithel, *Phys. Rev. Lett.* **107**, 103001 (2011).
- [43] A. Schwarzkopf, D. A. Anderson, N. Thaicharoen, and G. Raithel, *Phys. Rev. A* **88**, 061406(R) (2013).
- [44] N. Thaicharoen, A. Schwarzkopf, and G. Raithel, *Phys. Rev. A* **92**, 040701(R) (2015).
- [45] D. P. Fahey, T. J. Carroll, and M. W. Noel, *Phys. Rev. A* **91**, 062702 (2015).
- [46] M. Stecker, H. Schefzyk, J. Fortágh, and A. Günther, *New J. Phys.* **19**, 043020 (2017).
- [47] J. Grimm, M. Mack, F. Karlewski, F. Jessen, M. Reinschmidt, N. Sándor, and J. Fortágh, *New J. Phys.* **17**, 053005 (2015).
- [48] J. Grimm, M. Stecker, M. Kaiser, F. Karlewski, L. Torralbo-Campo, A. Günther, and J. Fortágh, *Phys. Rev. A* **96**, 013427 (2017).
- [49] R. Kosloff and D. Kosloff, *J. Comput. Phys.* **63**, 363 (1986).
- [50] U. V. Riss and H. D. Meyer, *J. Phys. B* **26**, 4503 (1993).
- [51] S. Sahoo and Y. K. Ho, *J. Phys. B* **33**, 2195 (2000).
- [52] T. F. Gallagher, *Rydberg Atoms* (Cambridge University Press, Cambridge, England, 1994).
- [53] I. I. Beterov, I. I. Ryabtsev, D. B. Tretyakov, and V. M. Entin, *Phys. Rev. A* **79**, 052504 (2009).
- [54] R. Feynman, J. Hollingsworth, M. Vennettilli, T. Budner, R. Zmiewski, D. P. Fahey, T. J. Carroll, and M. W. Noel, *Phys. Rev. A* **92**, 043412 (2015).
- [55] I. I. Ryabtsev, I. I. Beterov, D. B. Tretyakov, V. M. Entin, and E. A. Yakshina, *Phys. Usp.* **59**, 196 (2016).
- [56] C. Ates, T. Pohl, T. Pattard, and J. M. Rost, *Phys. Rev. A* **76**, 013413 (2007).
- [57] D. Petrosyan, *Phys. Rev. A* **88**, 043431 (2013).
- [58] D. Petrosyan, M. Höning, and M. Fleischhauer, *Phys. Rev. A* **87**, 053414 (2013).
- [59] J. M. McGuirk, D. M. Harber, J. M. Obrecht, and E. A. Cornell, *Phys. Rev. A* **69**, 062905 (2004).
- [60] J. M. Obrecht, R. J. Wild, and E. A. Cornell, *Phys. Rev. A* **75**, 062903 (2007).
- [61] A. Tauschinsky, R. M. T. Thijssen, S. Whitlock, H. B. van Linden van den Heuvell, and R. J. C. Spreeuw, *Phys. Rev. A* **81**, 063411 (2010).
- [62] H. Hattermann, M. Mack, F. Karlewski, F. Jessen, D. Cano, and J. Fortágh, *Phys. Rev. A* **86**, 022511 (2012).
- [63] D. Petrosyan, G. Bensky, G. Kurizki, I. Mazets, J. Majer, and J. Schmiedmayer, *Phys. Rev. A* **79**, 040304 (R) (2009).
- [64] S. D. Hogan, J. A. Agner, F. Merkt, T. Thiele, S. Filipp, and A. Wallraff, *Phys. Rev. Lett.* **108**, 063004 (2012).
- [65] L. Sárkány, J. Fortágh, and D. Petrosyan, *Phys. Rev. A* **92**, 030303(R) (2015).
- [66] L. Sárkány, J. Fortágh, and D. Petrosyan, *Phys. Rev. A* **97**, 032341 (2018).
- [67] D. Petrosyan, K. Mølmer, J. Fortágh, and M. Saffman, *New J. Phys.* **21**, 073033 (2019).
- [68] S. Bernon, H. Hattermann, D. Bothner, M. Knufinke, P. Weiss, F. Jessen, D. Cano, M. Kemmler, R. Kleiner, D. Koelle, and J. Fortágh, *Nat. Commun.* **4**, 2380 (2013).
- [69] H. Hattermann, D. Bothner, L. Y. Ley, B. Ferdinand, D. Wiedmaier, L. Sárkány, R. Kleiner, D. Koelle, and J. Fortágh, *Nat. Commun.* **8**, 2254 (2017).
- [70] M. Saffman, *J. Phys. B* **49**, 202001 (2016).